CONTRACT NO. DAHC04-69-C-0077
ARPA ORDER NO. 1462
PROGRAM CODE 9E30

TRANSIENT AND ASYMPTOTICALLY STEADY FLOW OF AN INVISCID, COMPRESSIBLE GAS PAST A CIRCULAR CYLINDER

by

GINO MORETTI

POLYTECHNIC INSTITUTE OF BROOKLYN

DEPARTMENT
of
AEROSPACE ENGINEERING
and
APPLIED MECHANICS

APRIL 1970

FINAL REPORT No. 70-29

TRANSIENT AND ASYMPTOTICALLY STEADY FLOW OF AN INVISCID, COMPRESSIBLE GAS PAST A CIRCULAR CYLINDER[+]

by

Gino Moretti[*]
Polytechnic Institute of Brooklyn
Graduate Center, Farmingdale, New York

ABSTRACT

A numerical analysis is made of the inviscid flow produced by a cylinder which accelerates from a state of rest to a constant, subsonic speed in a gas at rest. All features of the numerical solution are explained on physical grounds. Consequently, ways are suggested to computed steady subsonic flows around obstacles with a maximum accuracy and a minimum computational time.

[+]This research was supported by the Advanced Research Projects Agency of the Department of Defense and was monitored by U.S. Army Research Office-Durham, Box CM, Duke Station, Durham, North Carolina 27706, under Contract No. DAHC04-69-C-0077.

[*]Professor of Aerospace Engineering.

TABLE OF CONTENTS

TABLE OF CONTENTS

SECTION I

INTRODUCTION

Time-dependent computations have been used primarily as a device to obtain steady state solutions of gas dynamical problems. As such, they do not differ conceptually from the relaxation method[1,2]; no computed results, except the final ones, are to be interpreted physically. In principle, one can use a numerical technique which is consistent with the physico-mathematical model only in the limit, when all time derivatives vanish (see, for example, Refs. 3 and 13).

In the first impressive applications of the relaxation method[1], the computations (performed by hand) were constantly kept under the control of the analyst who, perhaps semi-consciously, would use his physical intuition to direct the work to a reasonable end. If the task is shifted to a machine which operates, uncontrolled, by brute force, most likely the results do not converge or converge to a physically unreasonable pattern. This can be said of relaxation methods and time-dependent techniques as well. So long as no physical meaning can be given to the time-dependent results as functions of time, physical intuition cannot be used to explain the origin and nature of troubles. Such vague terms as "nonlinear instability" are then used to mean that there is trouble but one does not know why.

I intend to show, by a detailed analysis of a particular problem, that time-dependent techniques may be devised which closely describe an actual time-dependent evolution; that errors,

generated by local inconsistencies of the numerical model with the physical model, propagate throughout the flow field according to physical laws; consequently, that troubles can be traced back to their point of origin; and finally, that the initial and boundary conditions are as important in the numerical treatment as they are in the physical phenomenon.

The problem chosen for analysis is the two-dimensional, inviscid compressible flow past a circular cylinder. The choice is justified by some interesting features of the flow, namely,

1) The cylinder may move at a subsonic speed. In this case, the steady state solution should cover the entire plane.

2) Under the above assumption, a local bubble of supersonic flow (relative to the cylinder) may form. In this case, one expects an imbedded shock.

3) If the cylinder moves at a supersonic speed, the perturbed region in a steady state is limited to a portion of the plane (behind the bow shock).

4) Under the above assumption, can a numerical solution be found which has all the characters of an inviscid flow, that is, without separation in the leeward side?

5) How does a steady pattern form when the cylinder takes on a constant speed starting from a state of rest?

In addition, the choice of a circular cylinder instead of another geometrical shape is justified by some simplification in the treatment of the wall points (which does not restrict the general conclusions). Finally, a similar problem has been considered by other authors[4,5,6] and myself[7]. Thus a critical

comparison can be made which confirms some of the conclusions of the present paper.

SECTION II

THE PHYSICAL PROBLEM

Consider a cylinder at rest in a gas at rest. Let the center of the cylinder start moving along a straight line (the x-axis), from right to left, with a velocity increasing from 0 to a maximum value, V_o. For example, let

$$\dot{x}_o = -V_o \sin\omega t \qquad (0 \leq t \leq \pi/2\omega) \tag{1}$$

where t is time and x_o is the abscissa of the center of the cylinder on the fixed x-axis. For $t > \pi/2\omega$, let the cylinder move at a constant speed along the x-axis. Asymptotically in time, a steady flow should be observable in a frame moving with the cylinder. At infinity, such flow should have a uniform velocity, V_o, and uniform values of the other physical parameters (all equal to their values in the gas at rest). We want to analyze the transient from a physical viewpoint first.

For consistency with the convention adopted in the numerical analysis, nondimensional symbols will be used. All pressures and densities are scaled to their values (p_∞, ρ_∞) in the gas at rest, all velocities are scaled to $\sqrt{p_\infty/\rho_\infty}$, all lengths are scaled to the radius of the cylinder, r_o, and all times are scaled to $r_o/\sqrt{p_\infty/\rho_\infty}$. In particular, the speed of sound in the gas at rest is equal to $\sqrt{\gamma}$ in nondimensional form, where γ is the ratio of specific heats. A pressure coefficient will be defined as:

$$C_p = \frac{p-1}{V_o^2/2} \tag{2}$$

Our arguments will be illustrated by two sets of sketches. One will depict the state of the flow at a given time on the plane of motion, by an isobar pattern. The cross-section of the cylinder will appear as in the upper part of Fig. 1. The other will show isobars, as functions of time, along the heavy line in the upper part of Fig. 1, which consists of

1) the x-axis in front of the cylinder,

2) the upper surface of the cylinder, and

3) the x-axis behind the cylinder.

As shown in the lower part of Fig. 1, the time axis runs horizontally from left to right. Lines AA and BB represent points A and B, respectively, in a frame moving with the cylinder.

Between BB and AA, $\zeta = \theta^{o}/100 - .9$. This strip represents the upper part of the cylinder. Above AA, where the x-axis in front of the cylinder is represented, $\zeta = -x - 0.1$. Below BB, where the x-axis behind the cylinder is represented, $\zeta = -x + 0.1$. In a steady state (with respect to the cylinder) the isobars are straight, horizontal lines. Any perturbation produced by the cylinder at any time $t > o$ is confined to the region bounded by the two characteristics issuing from A and B at t=0, unless they are overcome by a faster moving shock. The upper characteristic, AM, is defined by $d\zeta/dt = \sqrt{\gamma} + \dot{x}_o$, the lower one, BN, by $d\zeta/dt = -\sqrt{\gamma} + \dot{x}_o$. Therefore, once the cylinder moves at a constant speed $V (= M_o\sqrt{\gamma})$ both characteristics become straight lines, defined by

$$d\zeta/dt = -\sqrt{\gamma}\,(M_o \mp 1), \tag{3}$$

respectively.

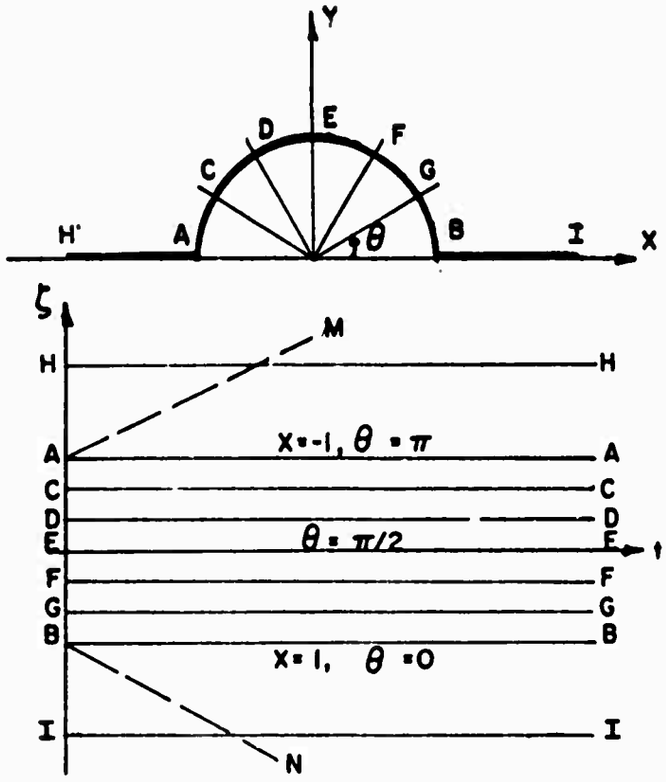

Fig. 1

When the cylinder starts moving to the left, the portion of the cylinder near A acts on the flow at rest as a piston and, in the first phase of the motion, the ensuing flow is, to all practical effects, one-dimensional. At a time,

$$t_A = \frac{2\sqrt{\gamma}}{(\gamma+1)\,|\dot{X}_o(0)|} = \frac{2\sqrt{\gamma}}{(\gamma+1)V_o\,\omega} \tag{4}$$

a shock builds up along the AM characteristic. Shortly thereafter, the one-dimensional shock reaches its peak strength. At $t_1 = \pi/2\omega$, when the cylinder starts moving at a constant speed, the pressure at A is approximately given by:

(5) $$p_A = \left(\frac{a}{\sqrt{\gamma}}\right)^{\frac{2\gamma}{\gamma-1}} = \left(1+\frac{\gamma-1}{2\sqrt{\gamma}}V_o\right)^{\frac{2\gamma}{\gamma-1}} \approx 1+\sqrt{\gamma}\,V_o$$

if $V_o \ll 1$. Thus

(6) $$C_{pA}(t_1) \approx 2\sqrt{\gamma}/V_o$$

The pressure behind the fully developed shock in the one-dimensional case is

(7) $$p = \frac{2\gamma M_s^2 - (\gamma-1)}{\gamma+1}$$

where M_s is the ratio between the modulus of the shock velocity in a fixed frame and the speed of sound in the gas at rest, $\sqrt{\gamma}$. The velocity of the gas relative to the shock is

(8) $$u_{rel} = V + \sqrt{\gamma}\,M_s$$

where V is the absolute velocity of the gas in a fixed frame. In front of the shock thus,

$$u_{rel} = \sqrt{\gamma}\,M_s$$

Behind the shock,

(9) $$u_{rel} = \sqrt{\gamma}\,M_s\,\frac{(\gamma-1)M_s^2+2}{(\gamma+1)M_s^2} = -V_o+\sqrt{\gamma}\,M_s$$

Therefore,

$$2M_s^2 - \frac{\gamma+1}{\sqrt{\gamma}}V_o M_s - 2 = 0$$

and

(10) $$M_s = \frac{1}{4}\left\{\frac{\gamma+1}{\sqrt{\gamma}}V_o + \sqrt{\frac{(\gamma+1)^2}{\gamma}V_o^2 + 16}\right\}$$

By substituting M_s from (10) into (7), simplifying for $V_o \ll 1$ and comparing with (5) or (6), one sees that the final pressure between piston and shock when a steady state is reached is practically the

same as the pressure at the beginning of the constant velocity phase of the piston motion, if V_o is small.

At B, the opposite phenomenon occurs. If B were a one-dimensional piston, its motion would produce an expansion wave and the pressure at B would be given by

$$p_B = \left(1 - \frac{\gamma-1}{2\sqrt{\gamma}} V_o\right)^{\frac{2\gamma}{\gamma-1}} \approx 1 - \sqrt{\gamma}\, V_o \tag{11}$$

Consequently, at B

$$C_{pB} = -2\sqrt{\gamma}\, / V_o \tag{12}$$

We can, thus, anticipate the existence of a first phase of the motion in which the front and the rear of the cylinder act independently as compressing and expanding pistons, respectively. In this phase, a shock, similar in strength to a one-dimensional shock, will form in front of A and surround the front of the cylinder. Its strength decreases as the $\theta=\pi/2$ line is approached; then the shock degenerates into a characteristic surface surrounding an expansion zone in the back of the cylinder.

At the same time, however, a compression wave is sent by A all along the cylinder towards the rear and an expansion wave is sent by B towards the front. As a result, the pressure decreases on the front of the body and increases on its back. The pressure distribution around the cylinder in the first phase of the motion is qualitatively shown in Fig. 2a. Soon after the motion starts, the compressed and expanded regions are practically antisymmetrical with respect to the $\theta=\pi/2$ line. The shadowed region corresponds to $C_p>0$. The pressure waves did not coalesce yet into a shock.

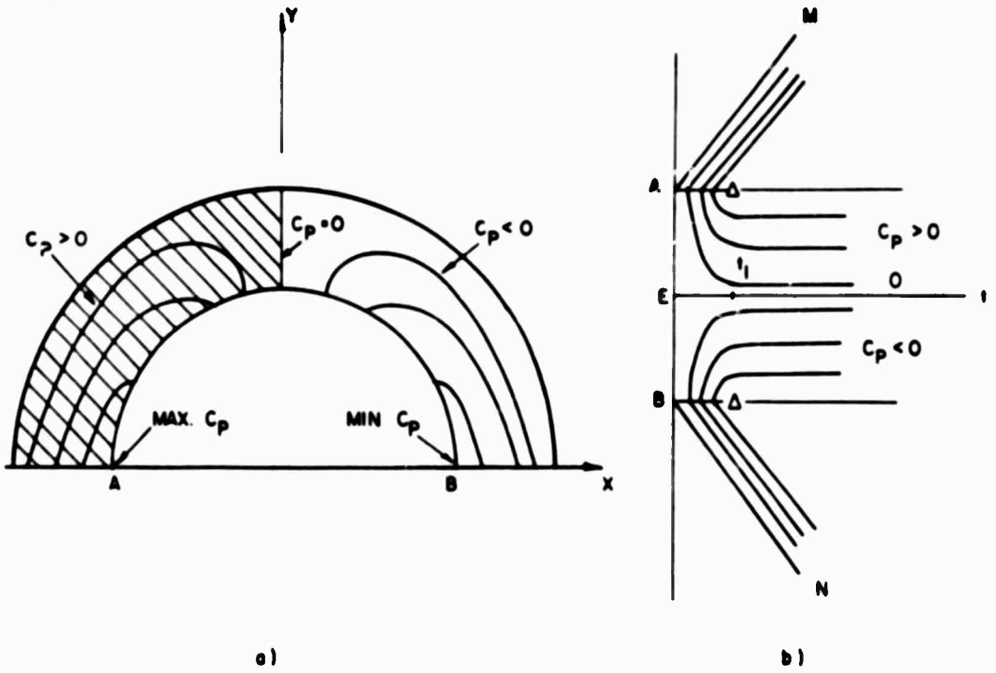

Fig. 2

The almost antisymmetric pattern evolves in time along the HAEBI line as shown in Fig. 2b.

The curvature of the walls acts against the effects described above. As soon as the acceleration vanishes, that is, at $t=t_1$, the pressure at A starts dropping and the pressure at B starts increasing. The effect is shown in Fig. 3 by the closing of some of the isobars. Note that the perturbations produced at J and L (that is, the points A and B of the circle at time t_1) propagate along the lines JK and LP, almost parallel to AM and BN, respectively. The effect above is still antisymmetric. However,

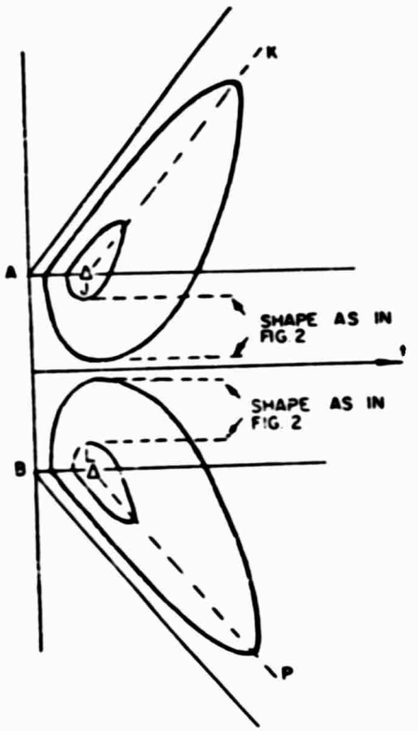

FIG. 3

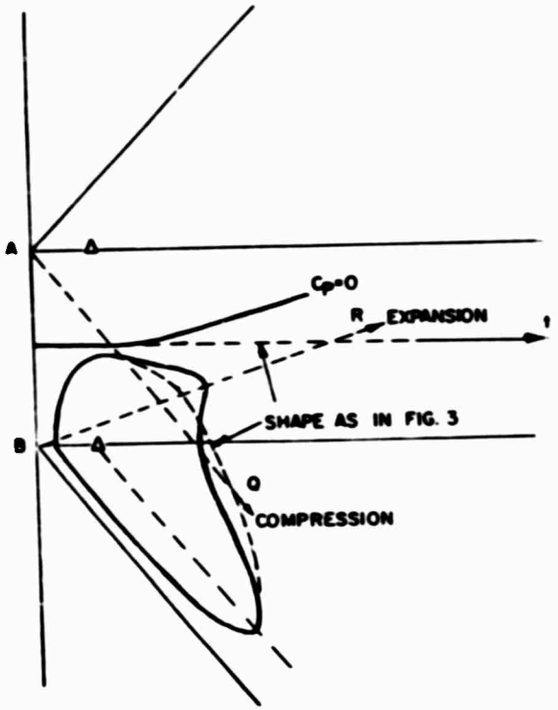

FIG. 4

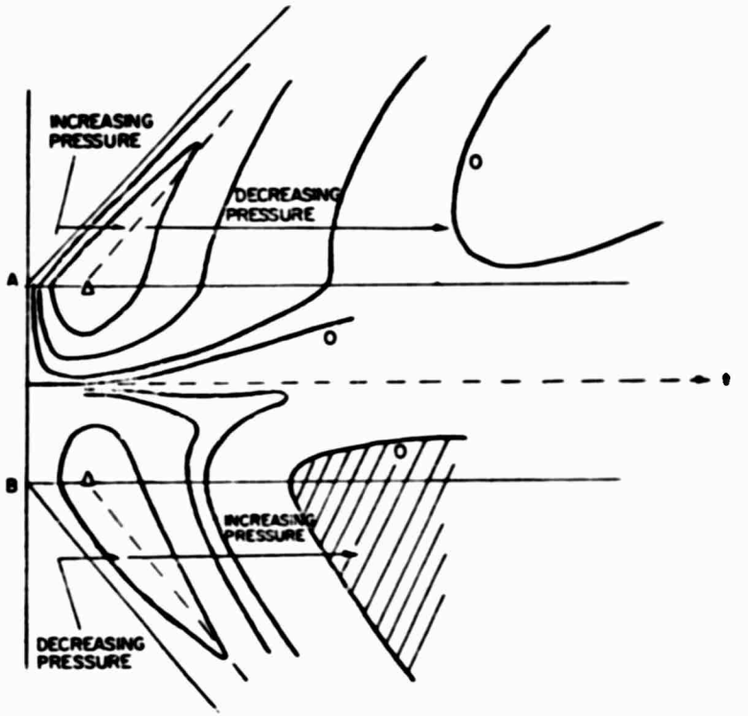

FIG. 5

another effect takes place meanwhile. The compressions generated along AJ and the expansions generated along BL propagate along the cylinder. As a consequence, the pressures to the right of the line AQ tend to increase, and the pressures to the right of the line BR tend to decrease. The isobars tend to bulge, as shown in Fig. 4. The effect is different in the front and back of the cylinder since the perturbations propagate at different speeds in opposite directions. The compression is moving faster than the expansion; thus, the changes in the isobar pattern is more impressive in the back side of the cylinder. The expanded zone tends to move forward, twisting the $C_p=0$ line out of symmetry, and a new compressed zone develops near point B (the shadowed region in Figs. 5 and 6).

In Fig. 6, note that most of the outer boundary is unaffected; indeed, it moves outwards at the speed of sound and cannot be reached by perturbations generated later on, other than fast-moving shocks.

In a steady state, at $V_o << 1$, (practically incompressible flow)

$$C_p = \frac{1}{r^3} \left(2 \cos 2\theta - \frac{1}{r^2}\right) \tag{13}$$

with r, θ polar coordinates with respect to the center of the cylinder and the x-axis. The isobars appear in a form, symmetrical to the $\theta=\pi/2$ line, shown in Fig. 7. The discussion above, and particularly Figs. 5 and 6, show how the transition from the antisymmetric pattern of Fig. 2 to the symmetric pattern of Fig. 7 can occur, in the vicinity of the body.

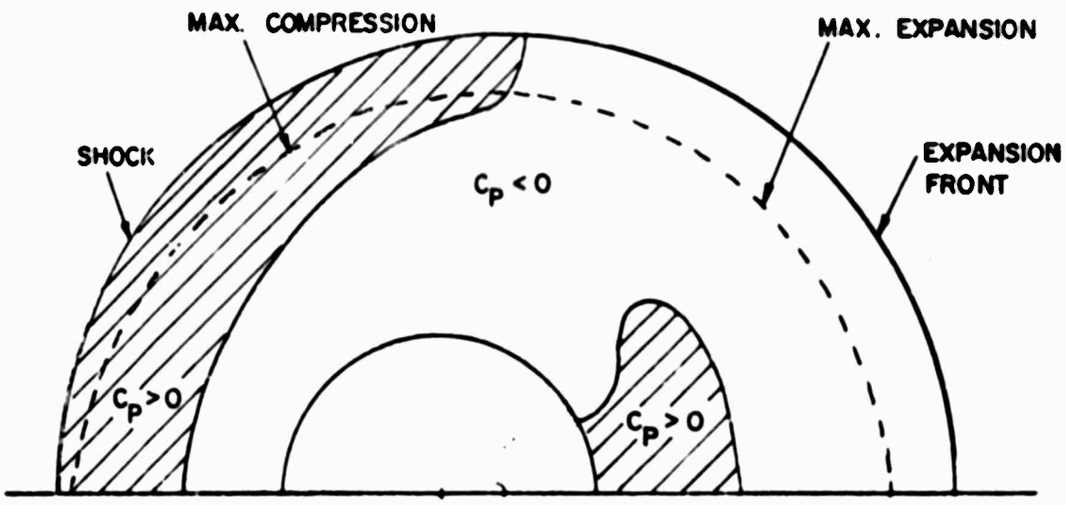
MAX. COMPRESSION
MAX. EXPANSION
SHOCK
EXPANSION FRONT
$C_p < 0$
$C_p > 0$
$C_p > 0$

FIG. 6

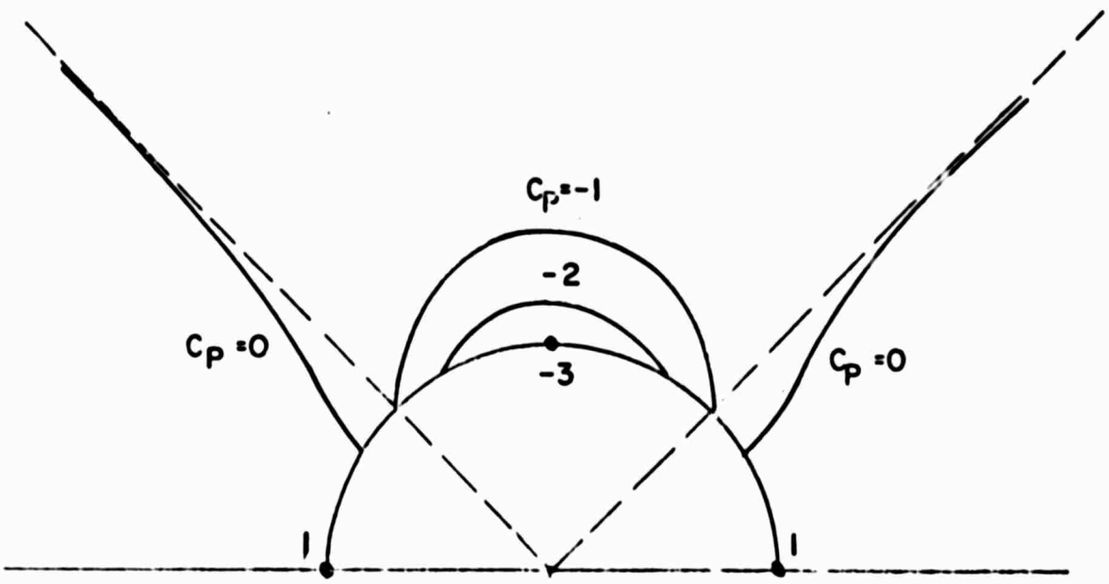
$C_p = -1$
-2
-3
$C_p = 0$
$C_p = 0$
1
1

FIG. 7

It must be clearly understood, however, that the complete pattern of Fig. 7 (that is, extending to infinity) is theoretically achieved only after an infinite time. Indeed, the pattern of Fig. 7 in the vicinity of the body is surrounded by an outward moving region which contains the remains of the original compression and expansion. As pointed out above, no further perturbation can reach and modify the initial wave front. Thus, at a finite time t a pattern similar to the one shown in Fig. 8 should appear.

Typical times and distances can be evaluated approximately by elementary means. Since the shock is weak, its velocity is practically the same as for a sound wave. Therefore, the outer boundary of the perturbed region can be found as the envelope of the perturbations issued by the body points at t=0. The envelope is defined parametrically by

$$[x+x_o(t)-\cos\varphi]^2 + [y-\sin\varphi]^2 = \gamma t^2 \tag{14}$$

if one assumes that the speed of sound in the perturbed region equals the speed of sound of the gas at rest and neglects the flow velocity. Elimination of φ between (14) and its derivative with respect to φ yields the equation of the envelope:

$$[x+x_o(t)]^2 + y^2 = (1+\sqrt{\gamma}\, t)^2 \tag{15}$$

which is a circle centered at $x= -x_o(t)$, $y=0$ and with a radius equal to $1 + \sqrt{\gamma}\, t$.

In a similar way, and under the same assumptions, the envelope of the perturbations issued by the body points at time t_1 (when the body starts moving at a constant speed) is found to be

$$[x+x_o(t)-x_o(t_1)]^2+y^2= [1+\sqrt{\gamma}\,(t-t_1)]^2 \tag{16}$$

that is, a circle centered at $x= -x_o(t)+x_o(t_1)=V_o(t-t_1)$, $y=0$ and with a radius equal to $1/\gamma\ (t-t_1)$. The two circles defined by (15) and (16) are shown in Fig. 8: they are marked FCD and GHL, respectively. The heavy-shadowed regions at the front and rear of the perturbed flow may contain pressure oscillations produced by compressive and expansive waves of decreasing strength, traveling almost periodically along the body as a result of the first compression and expansion; every time one of such waves arrives at either A or B, it sends a signal towards F or D, respectively, and these signals are alternate compressions and expansions of decreasing strength.

Let us consider now the case in which the cylinder accelerates to a higher speed, so high that a supersonic bubble is expected to appear at the top of the cylinder in the steady state. It is well-known experimentally that the return from supersonic to subsonic flow tends to take place abruptly, across a shock wave. The symmetry of the flow about the $\theta=\pi/2$ line, as in Fig. 7, is thus destroyed when a supersonic region exists. We can see how this happens by analyzing again the evolution of the flow in time.

It is evident from Figs. 5,6, and 8 that the transition from the initial, antisymmetrical pattern to the steady state pattern is characterized by a compression region growing about point B and moving towards the front of the cylinder. If high pressure differences exist between E and B, the forward moving pressure wave may coalesce into a shock, which will continue moving towards E until it reaches a position of equilibrium. In this case, Fig.8 is replaced by Fig. 9, where the imbedded shock is shown, starting

from the body at M. A qualitative sketch of the sonic line is also given.

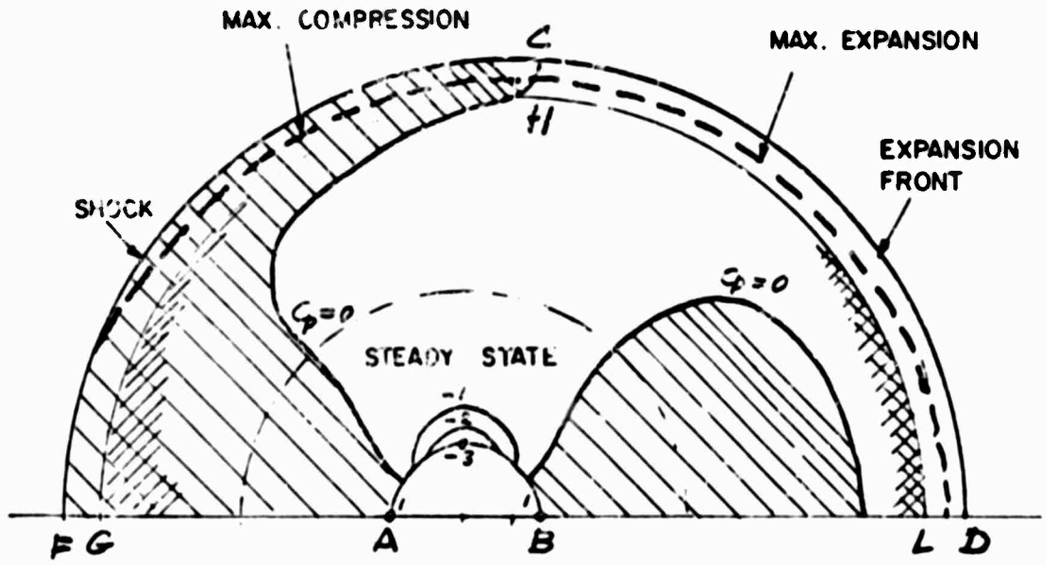

FIG. 8

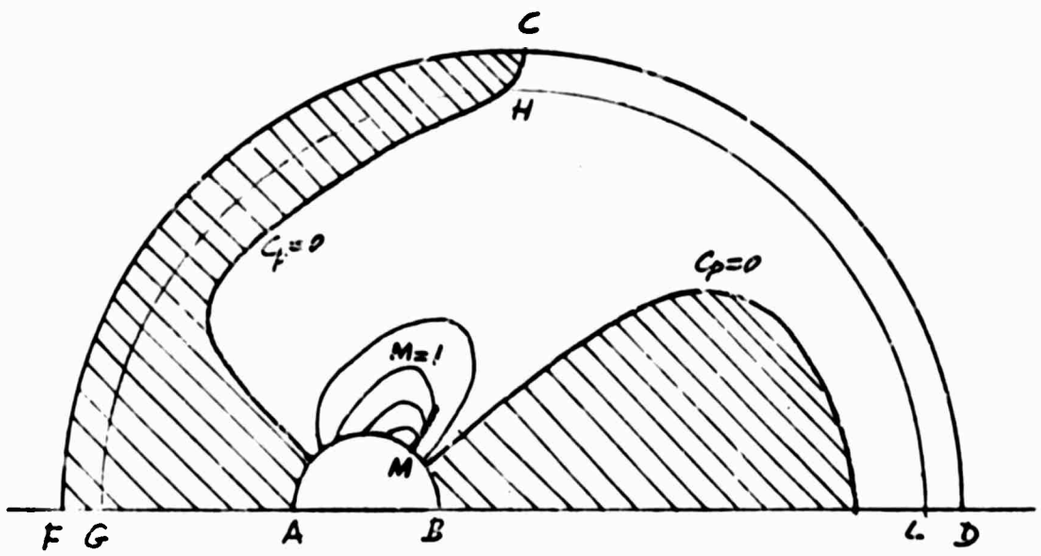

FIG. 9

SECTION III

OUTLINE OF A NUMERICAL TECHNIQUE

The numerical computation is performed in a region bounded by the cylinder and by an external boundary which is (except in the first phase of the motion) the line separating the perturbed flow by the outer flow at rest, with respect to the fixed frame. The numerical technique is composed of the following parts:

1. Computation of interior points.
2. Computation of points on the cylinder.
3. Computation of points on the outer boundary.
4. Test for coalescence of pressure waves.
5. Imbedded shock fitting.
6. Treatment of the initial phase of the motion.

SECTION IV

INTERIOR POINTS

To compute the interior points, the equations of motion for an inviscid, compressible flow are written in a polar frame, whose origin is located at the center of the cylinder and whose x-axis coincides with the x-axis of the fixed frame. Thus, the equations of motion are

$$
\left\{
\begin{aligned}
&P_t + uP_r + \frac{v}{r} P_\theta + \nu u_r + \frac{\gamma}{r} v_\theta + \gamma \frac{u}{r} = 0 \\
&u_t + uu_r + \frac{v}{r} u_\theta + \mathcal{J} P_r - \frac{v^2}{r} + \mathcal{X}_o \cos\theta = 0 \\
&v_t + uv_r + \frac{v}{r} v_\theta + \frac{\mathcal{J}}{r} P_\theta + \frac{uv}{r} - \mathcal{X}_o \sin\theta = 0 \\
&S_t + uS_r + \frac{v}{r} S_\theta = 0
\end{aligned}
\right. \tag{17}
$$

Here, u and v are the radial and transverse velocity components in the moving polar frame (that is, relative to the circle), $P=\ln p$, $\mathcal{J}=p/\rho$, $S=P-\gamma \ln \rho$.

In order to maintain a certain fineness of the mesh near the cylinder when the outer boundary moves away, a stretching of the r-coordinate is needed. The stretching is achieved by first normalizing the r-coordinate by means of the transformation

$$\zeta = \frac{r-1}{c-1} \tag{18}$$

where $r=c(\theta,t)$ is the polar equation of the moving boundary. Then a new set of variables (X,Y,T) is defined by

$$\begin{cases} \zeta = \tfrac{1}{2}\left[1+\dfrac{\tanh\alpha(X-0.5)}{\tanh(\alpha/2)}\right], \quad X = \tfrac{1}{2}+\dfrac{1}{2\alpha}\ln\dfrac{1+(2\zeta-1)\tanh(\alpha/2)}{1-(2\zeta-1)\tanh(\alpha/2)} \\ Y = \pi-\theta \\ T = t \end{cases} \tag{19}$$

where α is a function of time. Note that, at the body, $\zeta=0$ and $X=0$, and at the outer boundary, $\zeta=1$ and $X=1$. If the values of X are all equally spaced, with increasing α the values of ζ tend to accumulate in the vicinity of $\zeta=0$ and $\zeta=1$.

For any function f,

$$f_r = f_X X_\zeta \zeta_r, \quad f_\theta = -f_Y + f_X X_\zeta \zeta_\theta, \quad f_t = f_T + f_X (X_\zeta \zeta_t + X_\alpha \alpha_t) \tag{20}$$

In turn,

$$\zeta_r = \frac{1}{c-1}, \quad \zeta_\theta = -\zeta\zeta_r c_\theta, \quad \zeta_t = -\zeta\zeta_r c_t$$

$$X_\zeta = \frac{2\tanh(\alpha/2)}{\alpha}\,\frac{1}{1-(2\zeta-1)^2\tanh^2(\alpha/2)}, \quad X_\alpha = \frac{1-2X}{2\alpha}+\frac{2\zeta-1}{2\alpha}\,\frac{1-\tanh^2(\alpha/2)}{1-(2\zeta-1)^2\tanh^2(\alpha/2)} \tag{21}$$

The equations of motion in the (X,Y,T) space thus become

$$
\left.\begin{aligned}
&P_t+AP_X+BP_Y+\gamma(Cu_X-Dv_Y+Ev_X+F)=0\\
&u_T+Au_X+Bu_Y+GP_X+H=0\\
&v_T+Av_X+Bv_Y+JP_X+LP_Y+Q=0\\
&S_T+AS_X+BS_Y=0
\end{aligned}\right\} \tag{22}
$$

where

$$
\left.\begin{aligned}
&C=X_\zeta\zeta_r,\quad D=\frac{1}{r}=\frac{1}{1+\zeta(c-1)},\quad E=\frac{1}{r}X_\zeta\zeta_\theta\\
&F=\frac{u}{r},\quad G=\mathcal{J}C,\quad J=\frac{1}{r}\mathcal{J}X_\zeta\zeta_\theta,\quad L=-\frac{1}{r}\mathcal{J}\\
&B=-\frac{v}{r},\quad H=-\frac{v^2}{r}+\ddot{x}_o\cos\theta,\quad Q=\frac{uv}{r}-\ddot{x}_o\sin\theta\\
&A=X_\zeta\zeta_r[-\zeta c_t+u-\frac{v}{r}\zeta c_\theta]+X_\alpha\alpha_t
\end{aligned}\right\} \tag{23}
$$

To solve (22) numerically, a second-order accurate scheme is used. In the present case, I abandoned the scheme used in all my previous work in favor of a scheme recently used by MacCormack[8]. Numerical experiments performed on one-dimensional problems and on the blunt-body problem show that MacCormack's scheme yields the same accuracy with a simpler coding. The advantage is particularly strong in viscous flow problems and there are some minor advantages when imbedded shocks are present. There are no sizeable reductions in computational time, however, since the simpler scheme requires a double computation at each time step and this is almost equivalent to computing once the double set of first and second derivatives.

In the present scheme, a first set of intermediate values $\bar{f}^{\,k+1}_{n,m}$ at $t=(k+1)\Delta t$ is computed by the general formula

$$(24)\qquad \bar{f}^{k+1}_{n,m} = f^{k}_{n,m} + \left(A\,\frac{f^{k}_{n+1,m} - f^{k}_{n,m}}{\Delta X} + B\,\frac{f^{k}_{n,m+1} - f^{k}_{n,m}}{\Delta Y} + C\right)\Delta T$$

where

$$(25)\qquad f = \begin{bmatrix} P \\ u \\ v \\ S \end{bmatrix},\quad A = -\begin{bmatrix} A & \gamma C & \gamma E & 0 \\ G & A & 0 & 0 \\ J & 0 & A & 0 \\ 0 & 0 & 0 & A \end{bmatrix},\quad B = -\begin{bmatrix} B & 0 & -\gamma D & 0 \\ 0 & B & 0 & 0 \\ L & 0 & B & 0 \\ 0 & 0 & 0 & 0 \end{bmatrix},\quad C = -\begin{bmatrix} \gamma F \\ H \\ Q \\ 0 \end{bmatrix}$$

and the elements of A,B and C are computed at the point $X=n\Delta X$, $Y=m\Delta Y$. The final values $f^{k+1}_{n,m}$ are computed by the formula

$$(26)\qquad f^{k+1}_{n,m} = \frac{f^{k}_{n,m} + \bar{f}^{k+1}_{n,m}}{2} + \left(\bar{A}\,\frac{\bar{f}^{k+1}_{n,m} - \bar{f}^{k+1}_{n-1,m}}{\Delta X} + \bar{B}\,\frac{\bar{f}^{k+1}_{n,m} - \bar{f}^{k+1}_{n,m-1}}{\Delta Y} + C\right)\frac{\Delta T}{2}$$

where the elements of $\bar{A}$, $\bar{B}$ and $\bar{C}$ are based on the values $\bar{f}^{k+1}_{n,m}$.

It may be noted that the equations of motion are not formulated in conservation form. Let it be clearly stated that I never used the conservation form in any of my previous works either, since I do not see any strong reason for it[9,10].

SECTION V

BODY POINTS

The body geometry in the present problem is so simple that the body points can be computed by using an integration scheme similar to the one used for interior points. Obvious simplifications follow from the vanishing of u,X and X_α. Only one X-derivative, u_X is left in the equations. It is advisable to approximate it numerically by a three-point formula in both stages of the integration scheme. Better results seem to be obtained, however, if the method outlined in Ref. 10 is used. A Cartesian frame of reference is used at each body point; its ξ-axis is normal to

the wall and its η-axis is tangent to the wall. With respect to the cylinder, the (ξ,η) frame has a translational motion defined by a constant velocity, equal to the flow velocity at the body point, at time $(k+1)\Delta t$. Let $\tilde{u}$ and $\tilde{v}$ be the components of the flow velocity, relative to the cylinder, in the (ξ,η) frame. A characteristic equation in the (ξ,t) plane (which moves along with the ξ-axis, normally to itself) is written:

$$(27)\quad 0=\tilde{u}_{\star}-\frac{a}{\gamma}(P-P_{\star})-[av_{\theta}+\ddot{x}_{o}\cos\theta]\Delta t$$

where the values denoted by * are computed at $t=k\Delta t$ and at a point $A_{\star}$ defined by

$$(28)\qquad \xi_{\star}=(\tilde{u}-a)\Delta t,\quad \eta_{\star}=v\Delta t$$

and a, in (27) and (28), is the average speed of sound between the point to be computed and $A_{\star}$. Note that the zero in the left-hand side of (27) represents the vanishing u component at the body point.

The values at $A_{\star}$ must be interpolated between body points and interior mesh points at time $t=k\Delta t$. A linear interpolation seems to be sufficient.

SECTION VI

COMPUTATION AT THE OUTER BOUNDARY

For practical reasons the numerical analysis is started at $t=0$ over a region bounded by the rigid circle and another circle, centered at $x=-x_{o}(t_{o})$ and having a radius equal to $\sqrt{\gamma}\,t_{o}$, where $t_{o}\ll 1$. Such a circle is the wave front of the perturbation initiated at $t=0$, which propagates in all directions with the speed of sound of the gas at rest, $\sqrt{\gamma}$, and is left behind by the

moving circle. So long as $t<t_o$, the outer boundary is considered fixed and the values of the physical parameters on it are the values of the gas at rest (the velocity components, obviously, are not zero since they are relative to the moving circle). After $t=t_o$, the perturbed region must be allowed to spread outside of the initial boundary. From that moment on, the outer boundary is then considered as a moving shock.

Obviously, in its rear part such a line is not a shock at all but a sound wave, which travels with a velocity $\sqrt{\gamma} - \dot{x}_o \cos\varphi$ in the normal direction at each point (here φ is the angle between the normal to the wave and the x-axis). In the first phase of the motion mentioned above, the rear part of the "shock" actually is the leading edge of an expansion wave. However, the values of the physical parameters on the outer boundary and the velocity of the latter can be computed by considering the boundary as a shock all around since a sound wave is an infinitely weak shock and even a weak expansion can be considered as a shock of negative strength, to within an accuracy of the third order in M_n^2-1 (where M_n is the normal component of the Mach number, relative to the shock).

The computation of the shock proceeds as outlined in Ref. 11. The three Rankine-Hugoniot conditions, the conservation of tangential velocity, and one characteristic equation written for the interior of the computational region are sufficient to determine the shock velocity and the values of P,u,v, S behind the shock. A Cartesian frame of reference is used at each shock point; its ξ-axis is normal to the shock and its η-axis is tangent

to the shock, as it is at time t= (k+1)Δt. With respect to the cylinder, the (ξ,η) frame has a translational motion defined by a constant velocity, equal to the tangential component of the flow velocity at the shock at time (k+1)Δt. Let $\tilde{u}$ and $\tilde{v}$ be the components of the flow velocity, relative to the cylinder, in the (ξ,η) frame. Let N_1, N_2 and τ_1, τ_2 be the directive cosines of the ξ-axis and the η-axis, respectively, with respect to the r-axis and the normal to it, as they are at t=(k+1)Δt for the shock point to be computed. Then the tangential component of the velocity at the shock point is

$$\tilde{v}_s = -\dot{x}_o(\tau_1 \cos\theta - \tau_2 \sin\theta) \tag{29}$$

The normal component of the velocity at the shock point, in front of the shock is

$$\tilde{u}_{s_1} = -\dot{x}_o(N_1 \cos\theta - N_2 \sin\theta) \tag{30}$$

The normal component of the velocity relative to the shock, in front of it, is

$$V_{n\ rel_\infty} = \tilde{u}_{s_1} - W \tag{31}$$

where W is the shock velocity in the normal direction. With V_{nrel_∞} a relative normal Mach number is made,

$$M = V_{n\ rel_\infty} / \sqrt{\gamma} \tag{32}$$

and the first Rankine-Hugoniot equation yields the relative normal component of the velocity behind the shock,

$$V_{n\ rel} = V_{n\ rel_\infty} \frac{1 + \frac{\gamma-1}{2} M^2}{\frac{\gamma+1}{2} M^2} \tag{33}$$

The second and third Rankine-Hugoniot equations yield the density and pressure behind the shock,

$$\rho = \frac{V_{n\ rel_\infty}}{V_{n\ rel}} \tag{34}$$

$$p = \frac{(\gamma-1)\rho-(\gamma-1)}{\gamma+1-(\gamma-1)\rho} \tag{35}$$

From these equations, the values of P and S behind the shock are found:

$$P = \ln p \tag{36}$$

$$S = P-\gamma \ln \rho \tag{37}$$

A characteristic equation in the (ξ,t) plane (which moves along with the ξ-axis, normally to itself) is written:

$$\tilde{u}_s=\tilde{u}_\star+ \frac{a}{\gamma}(P-P_\star)+\left[a_\star\tilde{v}_{n_\star}-\chi_o\ (N_1\cos\theta-N_2\sin\theta)\right]\Delta t \tag{38}$$

where the values denoted by * are computed at $t=k\Delta t$ and at a point $A_\star$ defined by

$$\xi_\star = |\tilde{u}_s-a|\Delta t\ , \quad \eta = -\tilde{v}_s\Delta t \tag{39}$$

and a, in (38) and (39), is the average speed of sound between the point to be computed and $A_\star$. Since, on the other hand,

$$\tilde{u}_s=V_{n\ rel}+ W \tag{40}$$

the set of equations above can be used iteratively to determine all the unknowns contained therein.

The values at $A_\star$ must be interpolated between shock points and interior mesh points at time $t=k\Delta t$. The interpolation can be coded in many different ways. A well-formed shock, followed by a rather flat distribution of values, presents no difficulties.

However, for a shock generated by coalescence of compression waves, the distribution of values behind it is very steep. A simple linear interpolation tends to underestimate the pressure at A_*. Consequently, the computed value of P at the shock is too low and the shock does not build up strength. The errors generated at the shock propagate inside the computational region, producing oscillations which are not physically justified. This aberration has been detected in one-dimensional problems[9] and I suggested a different interpolation scheme which should work well under any circumstances. It should be noted that, if the linear scheme is used in a one-dimensional problem, the wiggles tend to disappear once the piston reaches a constant speed (because the piston keeps sending high-pressure signals towards the shock, thus giving it a chance to gain strength, eventually). Therefore, the aberration is disturbing but not lethal. In the present problem, instead, the pressure behind the shock must decrease, and strongly, in the second phase of the motion described above. The shock cannot correct its speed and shape, and the errors generated at the shock tend to grow bigger, inside the computational region, as the overall pressure decreases. The oscillations may eventually grow beyond control. It is thus imperative to use a better interpolation scheme in the shock computation; therefore, the scheme suggested in Ref. 9 has been adapted to the present two-dimensional problem.

SECTION VII

RADIAL STRETCHING

To complete the outline of the numerical scheme, a word must be spent on the definition of α in (19). If $\alpha << 1$, the relationship between α and X is almost linear. Therefore, equal intervals along the X-axis correspond to almost equal intervals between shock and body. With increasing distance between shock and body, the mesh size in the physical plane tends to grow too large. Now, there are two regions in the flow field where we must maintain a high radial resolution. One is a ring surrounding the body, where we want to achieve high accuracy since the values at the body are the most important from a practical standpoint. The other is the ring (FCDGHL) shown in Fig. 8, where the pressure changes rapidly from low to high values and to low values again for $\theta > \pi/2$ and has a similar, but reversed, behavior for $\theta < \pi/2$. Such changes are due to the fact that the initial perturbations (a strong compression coalescing into a shock and a strong expansion, respectively for $\theta > \pi/2$ and $\theta < \pi/2$) are followed by perturbations of the opposite kind. The thickness of the ring is of the order of the time spent to accelerate the body, multiplied by the speed of sound, that is, $\sqrt{\gamma}\,\pi/\omega$. Therefore, the nodes must concentrate in the vicinity of X=0 and X=1 and this justifies the choice of the stretching function (19). In addition, α should start increasing as soon as the first row of interior points reaches a distance d from the body which is considered as the greatest to be allowed for. From (18) and (19),

and forcing r-1=d when X=ΔX, we obtain

(41) $$\frac{d}{c-1} = \tfrac{1}{2}\left[1+ \frac{\tanh\alpha(\Delta X-.5)}{\tanh(\alpha/2)}\right]$$

Then

(42) $$\alpha_t = -\frac{d}{(c-1)^2}\, c_t \frac{2\tanh(\alpha/2)}{(\Delta X-.5)\left[1-\tanh^2\alpha(\Delta X-.5)\right]-2\tanh\alpha(\Delta X-.5)\operatorname{cosech}\alpha}$$

This equation can be conveniently used to increment α at each step in order to keep d practically constant. In (41) and (42), the values of c and c_t are assumed to be the ones on a typical radius, for example, on the x-axis in front of point A.

SECTION VIII

RESULTS FOR A FULLY SUBSONIC FLOW

To better understand how the flow develops in a simple case, where no imbedded shocks are present, I analyzed the case in which the Mach number of the uniform flow at infinity, relative to the circle, is equal to 0.1, and the circle accelerates slowly ($\omega=\pi$), making an attempt to perform an exhaustive study. A preliminary computation was made, with a simplified stretching in the radial direction. The value of d was taken as 0.05, and $t_o = 0.2$. The mesh had 7 intervals in the radial direction and 18 intervals circumferentially. Some of the resulting isobars are presented in Fig. 10. They show qualitative agreement with the pattern foreseen in Fig. 5. However, early wiggles indicate a poor resolution of the mesh. From a more detailed plot, which cannot be reproduced in a small scale, it appears that more and

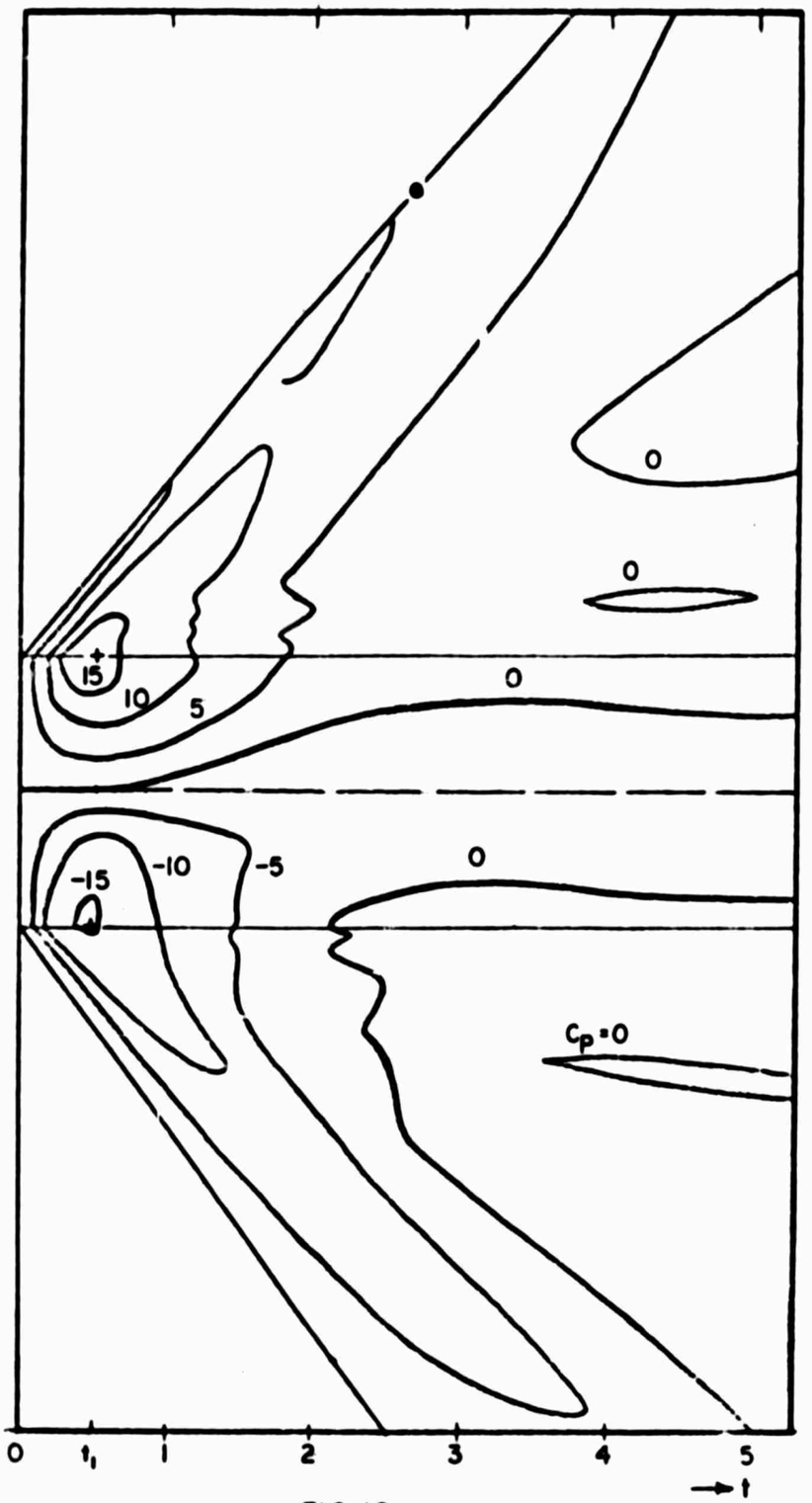

FIG. 10

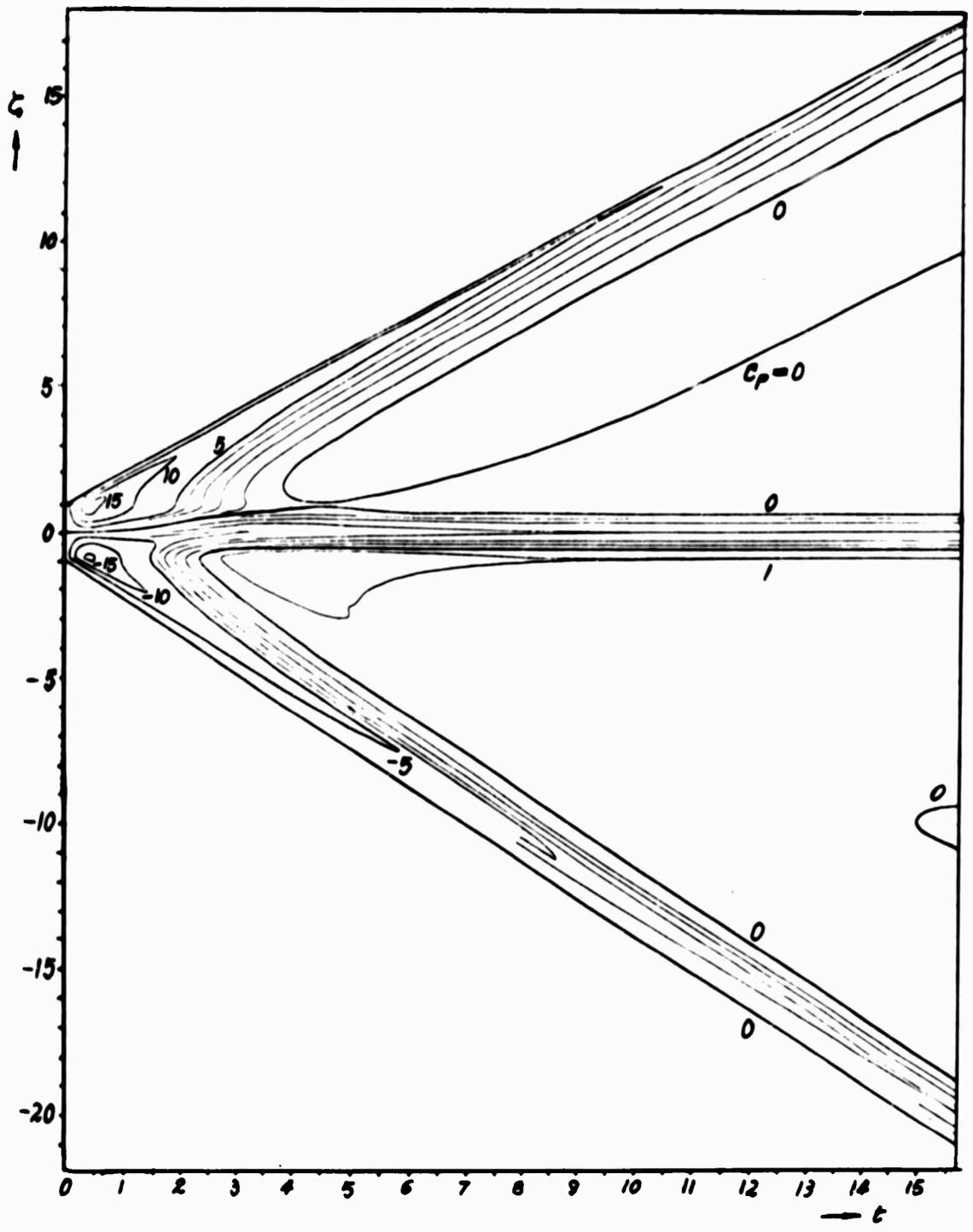
ζ
15
10
5
0
-5
-10
-15
-20
0 1 2 3 4 5 6 7 8 9 10 11 12 13 14 15
t
0
$C_p=0$
0
1
0
0
0
-5
-10
-15
-5

Fig. 11

more wiggles tend to develop at the back of the cylinder towards the last computed step (at t=5.25, after 300 cycles)*.

Increasing the number of radial intervals to 28 and using the sketchings defined above with d=0.05 definitely improves the calculation. The isobar pattern so obtained (Fig. 11) can be compared with Fig. 10. No wiggles appear and the pattern follows closely the predictions of Section II. Note that the C_p=0 line issuing from the top point on the cylinder almost reaches the forward stagnation point bringing a strong expansive effect, and then recedes towards its steady state location, 30^o above the stagnation point. After 650 cycles**, the pressure distribution along the circle is the one to be found in the steady state to within 1%. Figs. 12, 13 and 14 show in a different way how the steady state about the circle is reached. Fig. 12 is a plot of isobars in the plane of motion at the 400th cycle (t=5.06). This is about the time when the forward stagnation point undergoes the maximum expansion. Fig. 13 is a similar plot at the 700th cycle (t=10.36). The steady state is achieved within a circle centered at the center of the body and having a radius twice the radius of the body.

Finally, Fig. 14 is a similar plot at the 1000th cycle (t=15.66)+. The region within a circle centered at the center of the body is practically in a steady state. The result is consistent with the propagation of signals at a speed practically equal to the speed of sound in the gas at rest: if the steady

---

* One minute of CDC 6600 time.

** About 6 minutes of CDC 6600 time.

+ About eight minutes of CDC 6600 time.

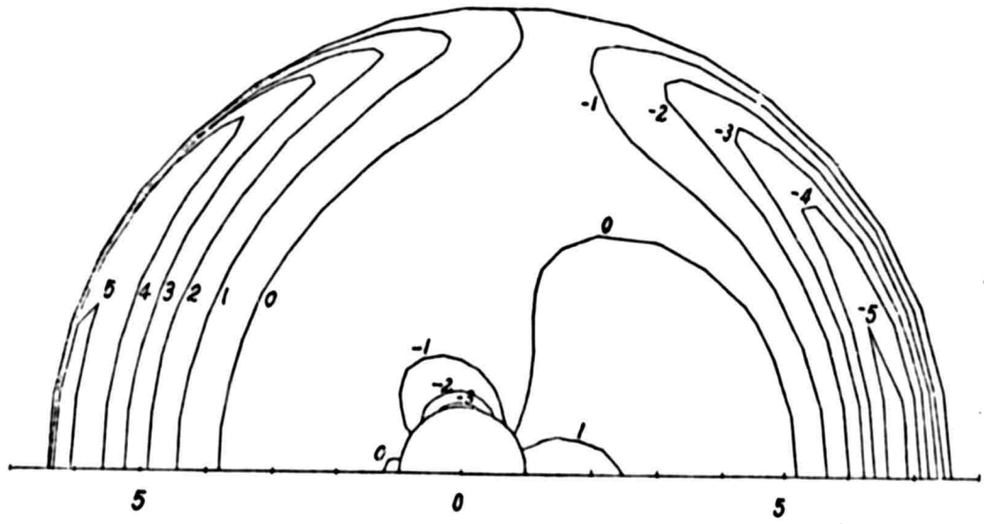

Figure 12

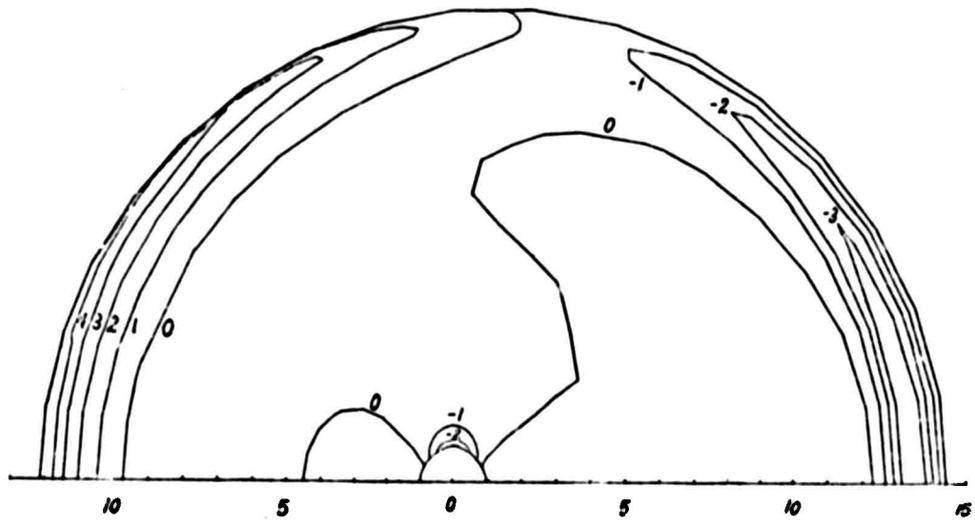

Figure 13

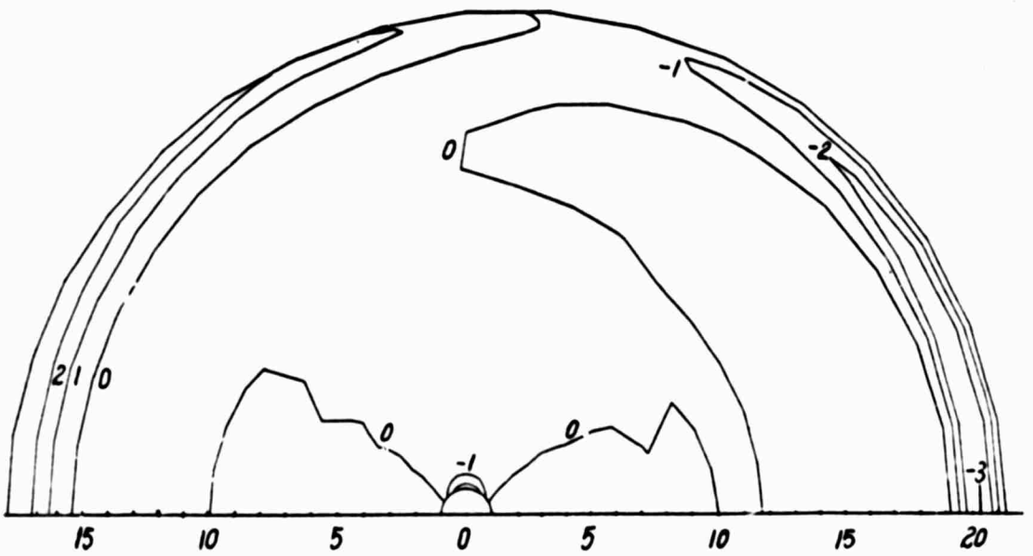

Figure 14

state front is at r=2 when t=10 and travels at a speed equal to $\sqrt{\gamma}$ = 1.183, it reaches r=8.7 at t=15.6.

The history of the pressure distribution on the symmetry line in front of the body is given by Fig. 15. The pressure coefficient is plotted as a function of r (the body is at the left and the initial perturbation front at the right) every 100 computational cycles. One can see how the initial, strong compression tends to form a shock. However, its tail is promptly reduced by the following expansion. Then a moderate compression builds up in the vicinity of the body and the steady state spreads outwards. The original compression and the following expansion are reduced in strength when the computation stops, but they are

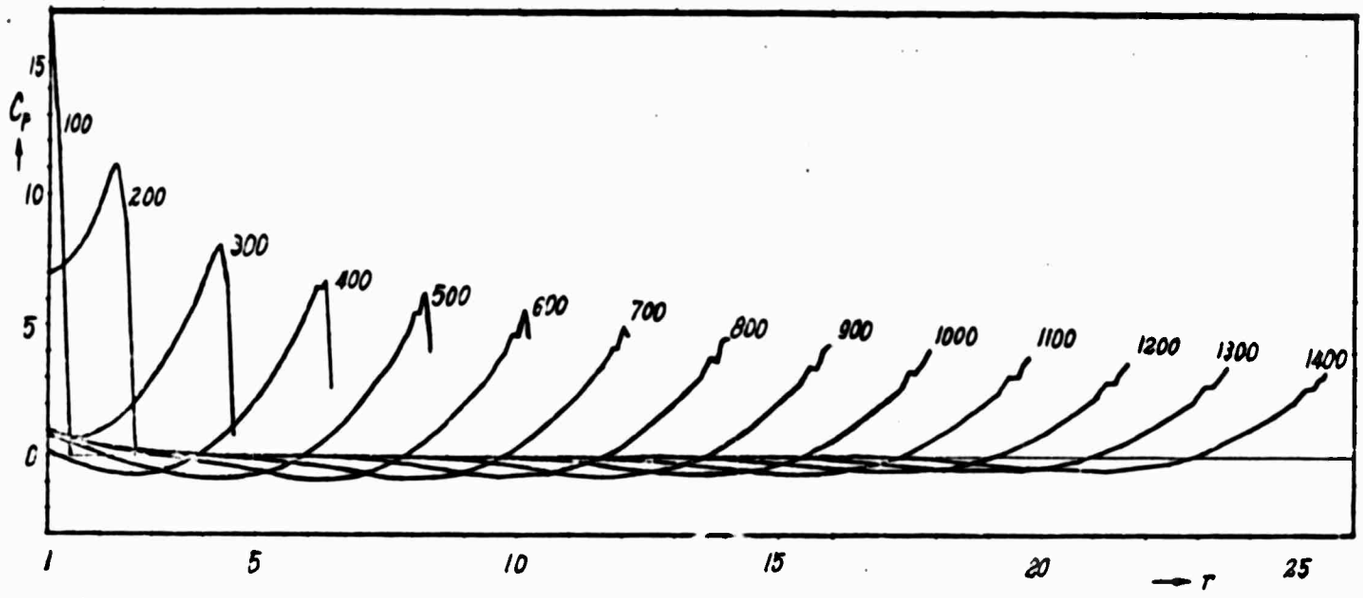

Figure 15

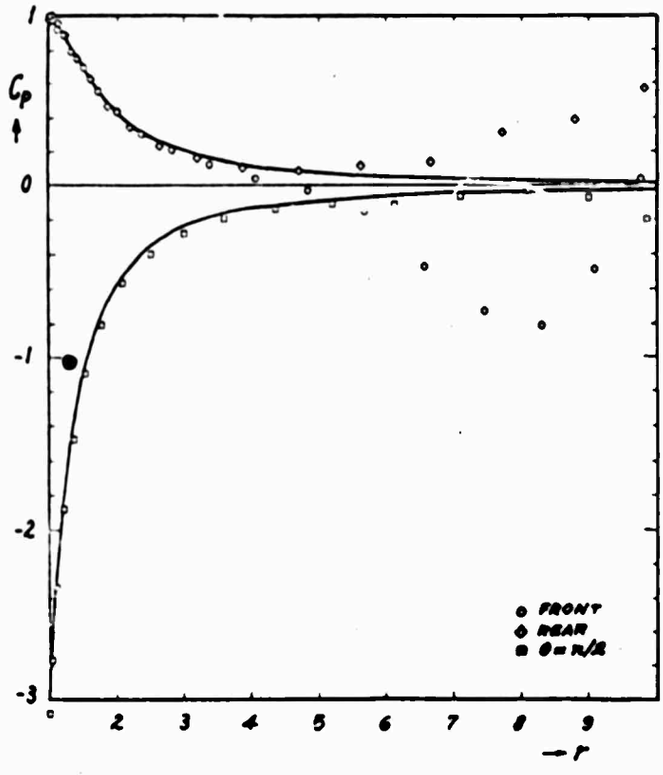

Figure 16

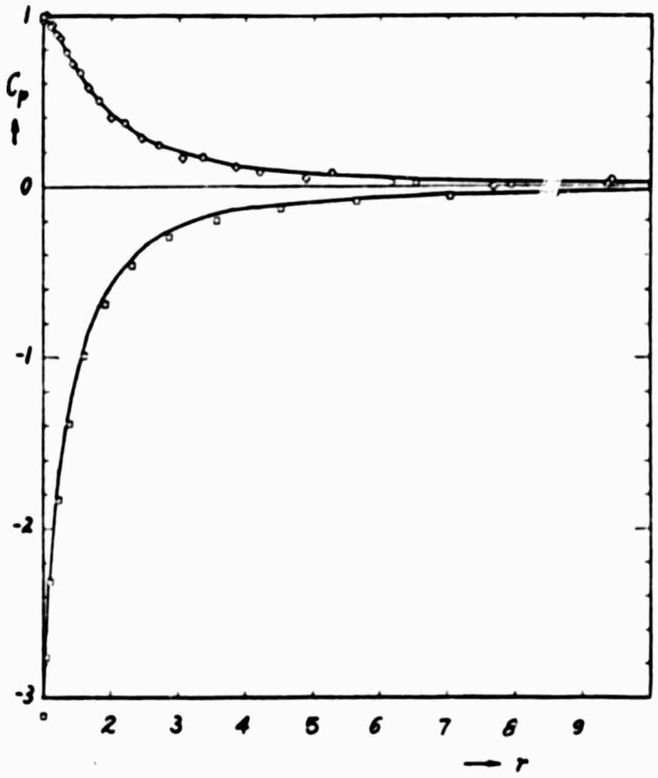

Figure 17

far from having been wiped out.

Figs. 16,17 and 18 confirm the fact that a steady state has been reached. The exact values of C_p in an incompressible, steady flow are given by

$$C_p = \frac{2\cos 2\theta}{r^3} - \frac{1}{r^4} \tag{43}$$

In Figs. 16, 17 and 18 the solid lines represent the exact values (43) on the front and rear stagnation lines and on the $\theta=\pi/2$ line. The computed values at the 700th cycle are plotted in Fig. 16 and the computed values at the 1000th cycle are plotted in Fig. 17. Not only is it clear that the steady state grows in size as explained above, but the accuracy of the results is proved. In a similar way, the solid line in Fig. 18 represents the exact values (43) along the body (r=1) and the computed values are plotted for a comparison.

Fig. 19 shows the pressure on the front stagnation line immediately behind the perturbation front, as a function of time. It appears that the shock starts building up at the time predicted by the one dimensional theory if the piston moves with the same law as the present body.

Let is be noted explicitly that the stretching of the radial coordinate and the number of nodes are necessary and strictly sufficient to get the results presented above, which I consider satisfactory from both a theoretical and a practical standpoint. If fewer nodes are taken in the outer ring, wiggles appear in the far field almost simultaneously with the beginning of the steady flow in the near field. The wiggles tend to move inwards as time increases and eventually they perturb the entire steady state

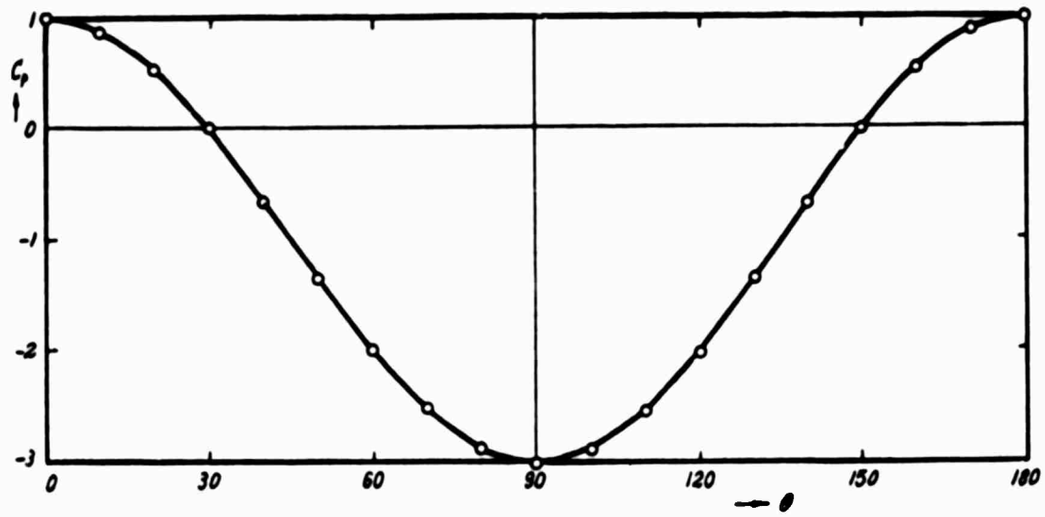

Figure 18

region.

In conclusion, we can issue a statement about the minimum computational time needed for determining the steady state at the surface of the body. Starting at the instant at which the acceleration of the cylinder stops, one should let the expansion wave travel all the way from the rear stagnation point to the fore stagnation point and then again travel all the way back to the rear stagnation point. The slowest speed of the wave is given by the difference between the speed of sound and the maximum modulus of the tangential velocity component. The latter is reached at $\theta = 90^{\circ}$ and is, according to the Rayleigh-Jantzen second order approximation for compressible flow (Ref. 14)

$$|v_{max}| = V_{\infty}(2 + \frac{7}{6} M_{\infty}^{4})$$

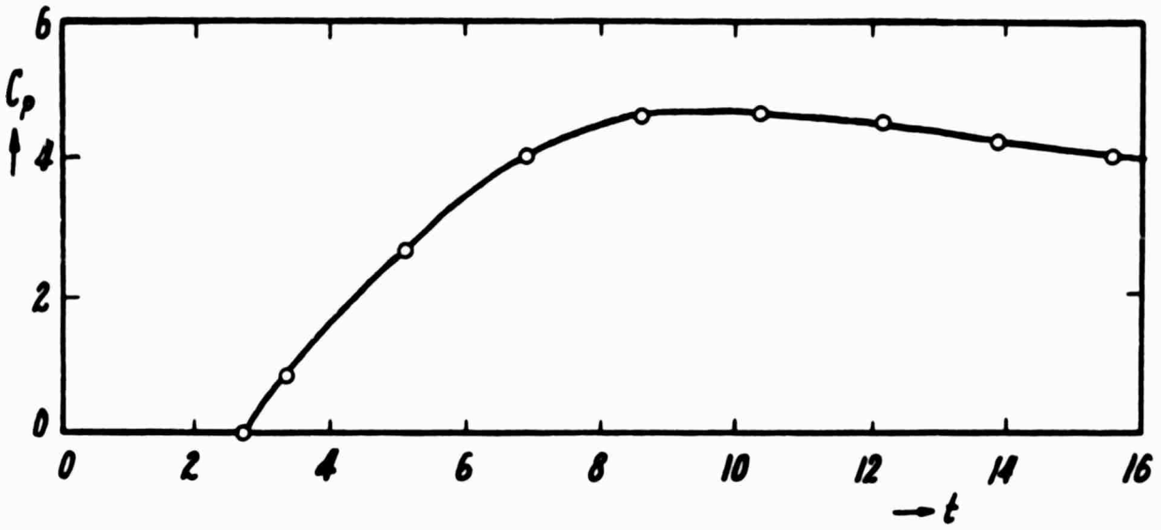

Figure 19

The steady state, thus, starts building up at the surface of the cylinder approximately at

$$t=t_1+\frac{2\pi}{\sqrt{\gamma}\left[1-M_\infty\left(2+\frac{7}{6}M_\infty^2\right)\right]} \tag{44}$$

if the speed of sound around the cylinder is considered equal to the speed of sound at infinity.

In the present case, $M_\infty = .1$, $t_1 = .5$ and $t \approx 7.2$. With a safety factor of 1.5, one can safely interrupt the computation at t=10, that is, after 700 computational cycles (about 6 minutes of CDC 6600 time).

For a cylinder one meter in diameter ($x_{ref} = .5$) accelerating to M= .1 in a standard atmosphere at sea level (a_∞=360 m/sec), $t_{ref} = .00164$. Then the physical time corresponding to t=10 equals .0164 sec. The ratio t between computational time and real time

is

$$t = \frac{360}{.0164} = 22{,}000 \tag{45}$$

In the present computations, the safety coefficient applied to the Courant-Friedrichs-Lewy stability formula was taken substantially lower than necessary, and the size of the initial region substantially smaller than the distance of formation of the shock wave. By relaxing both conditions, one should be able to reduce the computation time to about 4 minutes, thus reducing t to about 15,000. This seems to be a lower boundary for t, with the present generation of computers.

SECTION IX

A CRITICAL SURVEY OF OTHER APPROACHES TO THE PROBLEM

At this stage, we have a complete analysis of the transition from the incipient motion to a steady state regime and a consistent matching of the physical evolution with its numerical description. Such a physically oriented study may also help us in judging the reliability of other numerical treatments of the steady state problem, all generally ascribed to the category of "time-dependent calculations".

A) The flow relative to the cylinder is studied in a frame fixed to it. An external boundary, also fixed with respect to the cylinder, is chosen arbitrarily. It is assumed that the flow parameters on such a boundary are those of the uniform flow at infinity. An arbitrary initial distribution of values is assumed in the computational region and the unsteady flow is computed. Such an approach, which seems to have been popular some years ago, was supported by the belief that, since the external boundary is taken at a respectable distance from the body, the conditions on it are, to all practical purposes, the same as at infinity (see, for example, Ref. 5). I have expressed my disagreement in Ref. 12. Here I wish to strengthen it on the light of the analysis above. We have seen that the steady state results from the interplay of signals travelling around the body and <u>outwards</u>. We have seen the disastrous effects on the near field of perturbations proceeding inwards from the far field. Now, in the first phases of a computation like the one described in this section, the signals from the body travel towards the outer boundary and cannot get out.

SECTION IX

A CRITICAL SURVEY OF OTHER APPROACHES TO THE PROBLEM

At this stage, we have a complete analysis of the transition from the incipient motion to a steady state regime and a consistent matching of the physical evolution with its numerical description. Such a physically oriented study may also help us in judging the reliability of other numerical treatments of the steady state problem, all generally ascribed to the category of "time-dependent calculations".

A) The flow relative to the cylinder is studied in a frame fixed to it. An external boundary, also fixed with respect to the cylinder, is chosen arbitrarily. It is assumed that the flow parameters on such a boundary are those of the uniform flow at infinity. An arbitrary initial distribution of values is assumed in the computational region and the unsteady flow is computed. Such an approach, which seems to have been popular some years ago, was supported by the belief that, since the external boundary is taken at a respectable distance from the body, the conditions on it are, to all practical purposes, the same as at infinity (see, for example, Ref. 5). I have expressed my disagreement in Ref. 12. Here I wish to strengthen it on the light of the analysis above. We have seen that the steady state results from the interplay of signals travelling around the body and <u>outwards</u>. We have seen the disastrous effects on the near field of perturbations proceeding inwards from the far field. Now, in the first phases of a computation like the one described in this section, the signals from the body travel towards the outer boundary and cannot get out.

The boundary sends signals inwards, which have very little to do with the outgoing waves. Indeed, such a boundary does not act as a rigid wall but it does not act as an infinite capacity where the pressure is constant since velocity and entropy are also kept constant on it. Consequently, one may expect to find an initial stage in which the results in the near field tend to approach the steady state solution, followed by a second stage of increasing inaccuracy.

A computation of this kind (assuming local consistency of the numerical scheme with the equations of inviscid unsteady motion) is surely a time-dependent one. However, it does not converge to the desired steady state pattern since it describes a problem with boundary conditions different from the ones consistent with the time-dependent evolution of a flow extending to infinity. In certain cases, the results are deceptively smooth. This is due to the presence of artificial viscosity in the numerical scheme. Clearly, there is no reason for the results of a dissipative calculation to be consistent with the time solution of an inviscid problem.

B) The infinite field about the obstacle is mapped onto a finite computational region by means of a stretching of coordinates in the radial direction. Again, arbitrary initial conditions are assumed. I proposed this technique in Ref. 12 and some applications were made in Ref. 7. By so doing, uniform values can be imposed on the outer boundary since the latter is actually at an infinite distance in the physical plane, and in principle, it is reached by outgoing waves only at $t=\infty$. At the light of the present study,

it is clear that a steady state tends to build up in the vicinity of the body but the computation eventually becomes unstable. Indeed, the spacing between nodes increases from the body to infinity. The resolution is extremely poor where it should be very high (within the ring which follows the initial perturbation front). In addition, in our exercise reported in Ref. 7, we assumed impulsive initial conditions. The initial phase of the motion, thus, was characterized by very strong perturbations. The technique was unable to handle shocks. As a consequence, the unsteady outgoing ring was full of numerical oscillations. As soon as these entered the region of poor resolution, they started feeding errors inwards. The flow, which had reached an almost perfect pressure distribution near the body after 1000 computational steps, was competely destroyed at step 2000. We can see now that the instability of the computation is explained again by inconsistency of the numerical analysis with the physical pattern. The same code, with initial conditions given by the incompressible, steady flow field, went through 2000 cycles with no symptoms of deterioration and errors less than 0.0002. It should also be noted that very good results in the vicinity of a body can be obtained by mapping the infinite physical field onto a finite computational field and letting the body start from rest, in those cases where no shocks build up along the perturbation front. Obviously, the computation is to be halted where the steady state is reached near the body and before the poor far field resolution damages the near field. Problems of this nature will be discussed in a forthcoming paper by B. Grossman.

C) Finally, the computation presented in Ref. 6 consists of assuming impulsive initial conditions and starting at a slightly later time. A perturbation front, in the form of a shock wave, similar to the one described in this report, is assumed around the body and let to expand. Unfortunately, an initial flow field must be defined between shock and body. Such a definition is bound to be arbitrary (in the present study, instead, the initial conditions are not arbitrary). The results presented in Ref. 6 are not so detailed to allow an analysis as minute as in this report. However, in the light of the present analysis, it appears that the initial abitrariness is forever trapped within the computational region and it should eventually damage the steady state around the body when the latter tends to spread outwards. By proceeding as in Ref. 6, it seems to be difficult to stop the calculation at the right time because there is no criterion available to determine whether and when a steady flow is reached in the vicinity of the body. The Author circumvents the onset of instabilities by using a low order integration scheme and numerical dissipation, two devices which I do not recommend.

SECTION X

REFERENCES

1. Southwell, R.V., Relaxation Methods in Theoretical Physics, Oxford, 1946.
2. Hayes, W.D. and Probstein, R.F., Hypersonic Flow Theory, Vol.I, page 438, Academic Press, New York, 1966.
3. Crocco, L., A Suggestion for the Numerical Solution of the Steady Navier-Stokes Equations, AIAA J., 3, 1824, 1965.
4. Evans, M.W. and Harlow, F.H., Calculation of Unsteady Supersonic Flow Past a Circular Cylinder, ARS J., January 1959, page 46.
5. Magnus, G., Gallaher, W., and Yoshihara, H., Inviscid Supercritical Airfoil Theory, AGARD Specialist' Meeting on Transonic Aerodynamics, Paris 18-20 September 1968.
6. Kentzer, C., Computations of Time Dependent Flows on an Infinite Domain, AIAA 8th Aerospace Sciences Meeting, New York, 1970, Preprint.
7. MacKenzie, D., and Moretti, G., Time Dependent Calculation of the Compressible Flow About Airfoils, AGARD Specialist' Meeting on Transonic Aerodynamics, Paris, 18-20 September 1968.
8. MacCormack, R.W., The Effect of Viscosity in Hypervelocity Impact Cratering, AIAA 7th Aerospace Sciences Meeting, Paper No. 69-354, 1969.
9. Moretti, G.,A Critical Analysis of Numerical Techniques: The Piston-Driven Inviscid Flow, PIBAL Report No. 69-25, July 1969.

10. Moretti, G., The Choice of Time-Dependent Technique in Gas Dynamics, PIBAL Report No. 69-26, July 1969.

11. Moretti, G. and Abbett, M., A Time-Dependent Computational Method for Blunt Body Flows, AIAA J., 4, 2136, 1966.

12. Moretti, G., Importance of Boundary Conditions in the Numerical Treatment of Hyperbolic Equations, Phys. Fluids, Supplement II, II-13, 1969.

13. Lifshitz,Yu.B., The Computation of Transonic Flow Past a Symmetric Profile, Mekh. Dz i Gaz. page 52, 1969.

14. Howarth, L.,(editor), Modern Developments in Fluid Dynamics, High Speed Flow, Page 275, Oxford 1953.

Unclassified
Security Classification

DOCUMENT CONTROL DATA - R & D

(Security classification of title, body of abstract and indexing annotation must be entered when the overall report is classified)

1. ORIGINATING ACTIVITY (Corporate author)
Polytechnic Institute of Brooklyn
Dept. of Aerospace Engrg. & Appl. Mechanics
Route 110, Farmingdale, New York 11735

2a. REPORT SECURITY CLASSIFICATION
Unclassified

2b. GROUP

3. REPORT TITLE

TRANSIENT AND ASYMPTOTICALLY STEADY FLOW OF AN INVISCID, COMPRESSIBLE GAS PAST A CIRCULAR CYLINDER

4. DESCRIPTIVE NOTES (Type of report and inclusive dates)

5. AUTHOR(S) (First name, middle initial, last name)
Gino Moretti

6. REPORT DATE	7a. TOTAL NO. OF PAGES	7b. NO OF REFS
April 1970	41	14

8a. CONTRACT OR GRANT NO	9a. ORIGINATOR'S REPORT NUMBER(S)
DAHC04-69-C-0077	
b. PROJECT NO	PIBAL REPORT NO. 70-20
c. ARPA Order No. 1442	9b. OTHER REPORT NO(S) (Any other numbers that may be assigned this report)
d. Program Code 9E30	

10 DISTRIBUTION STATEMENT

Distribution of this document is unlimited.

11 SUPPLEMENTARY NOTES	12 SPONSORING MILITARY ACTIVITY
	U.S. Army Research Office-Durham Box CM Duke Station, Durham, N. Carolina

13 ABSTRACT

A numerical analysis is made of the inviscid flow produced by a cylinder which accelerates from a state of rest to a constant, subsonic speed in a gas at rest. All features of the numerical solution are explained on physical grounds. Consequently, ways are suggested to computed steady subsonic flows around obstacles with a maximum accuracy and a minimum computational time.

DD FORM 1 NOV 65 1473

Unclassified
Security Classification

14. KEY WORDS	LINK A		LINK B		LINK C	
	ROLE	WT	ROLE	WT	ROLE	WT
Numerical techniques Time-dependent techniques Subsonic flow past a cylinder						